Cloud and Water Vapor Feedbacks to the El Niño Warming: Are They Still Biased in CMIP5 Models?

Lin Chen[1, 2], Yongqiang Yu[1], De-Zheng Sun[3]

1 LASG, Institute of Atmospheric Physics, Chinese Academy of Sciences, China

2 University of Chinese Academy of Sciences, China

3 Cooperative Institute for Environmental Studies/University of Colorado &NOAA/Earth System Research Laboratory, Boulder, Colorado, USA.

Submitted to J. Climate

Aug 2, 2013

Revised on Jan. 6

Corresponding author address: Dr. Yongqiang Yu, LASG, Institute of Atmospheric Physics, Chinese Academy of Sciences, No. 40, Hua Yan Li, Beijing 100029, China.

Email: yyq@lasg.iap.ac.cn

Abstract

Previous evaluations of model simulations of the cloud and water vapor feedbacks in response to El Niño warming have singled out two common biases in the Phase 3 of Coupled Model Inter-comparison Project (CMIP3) models: an underestimate of the negative feedback from the shortwave radiation forcing of clouds (SWCRF) and an overestimate of the positive feedback from the greenhouse effect of water vapor. Here we check whether these two biases are alleviated in the Phase 5 of Coupled Model Inter-comparison Project (CMIP5) models. While encouraging improvements are found, particularly in the simulation of the negative SWCRF feedback, the biases in the simulation of these two feedbacks remain prevalent and significant. It is shown that bias in the SWCRF feedback correlates well with biases in the corresponding feedbacks from precipitation, large-scale circulation and longwave radiation forcing of clouds (LWCRF). By dividing CMIP5 models into two categories—high score models (HSM) and low score models (LSM)—based on their individual skills of simulating the SWCRF feedback, we further find that ocean-atmosphere coupling generally lowers the score of the simulated feedbacks of water vapor and clouds, but the LSM is more affected by the coupling than the HSM. We also find that the SWCRF feedback is simulated better in the models that have a more realistic zonal extent of the equatorial cold tongue, suggesting that the continuing existence of an excessive cold tongue is a key factor behind the persistence of the feedback biases in models.

1. Introduction

Cloud and water vapor are major modulators in climate system and strongly influence both the global circulation and energy balance through their radiative effects (Manabe and Wetherald 1967; Hartmann and Short 1980; Harrison et al. 1990; Kiehl and Trenberth 1997; Soden 1997; Houghton et al. 2001; Stephens 2005). The climate sensitivity to the rise of the man-made greenhouse gases in the atmosphere depends critically on the feedbacks from water vapor and clouds. However, the feedbacks from cloud and water vapor are considered as the largest source of uncertainty in climate predictions (Bony and Dufresne 2005; Randall et al. 2007). Therefore, assessing the accuracy and narrowing the uncertainties of the cloud and water vapor feedbacks in current leading climate models is of obvious importance. Indeed, persistent efforts have been made in this regard (Cess et al. 1990; Sun and Held 1996; Bony and Dufresne 2005; Stephens 2005; Bony et al. 2006; Lin 2007; Zhu et al. 2007; Soden et al. 2008; Sun et al. 2009, hereafter referred to as Sun2009).

Work on the evaluation of the feedbacks from water vapor and clouds have employed two main methodologies. The first one involves examining the response of cloud and water vapor in different models to a prescribed or model predicted global warming (Cess et al. 1990, 1996; Soden and Held 2006; among others). These studies have revealed that the cloud feedbacks differ greatly among models while the globally averaged feedback from water vapor in the models follows that of a constant relative

humidity model. As noted by Sun2009, however, these results have neither pointed out which model has the right cloud feedback nor ruled out the possibility that all the models have a similar bias in water vapor feedback. In addition, a uniform increase in the SST is often used to examine the response of cloud and water vapor to global warming in models. But there is uncertainty with the spatial pattern of global warming. For one thing, the surface temperature is not likely to increase uniformly across the globe (Xie et al. 2010).

Another methodology used to examine the cloud and water vapor feedbacks in climate models involves examining the response of cloud and water vapor to SST changes on the time scales of El Niño-Southern Oscillation (ENSO) (Sun et al. 2003, 2006, 2009; Lloyd et al. 2009, 2011, 2012; among others). By comparing the response of cloud and water vapor to the ENSO forcing in nature with that in Atmospheric Model Inter-comparison Project (AMIP) simulations by some leading climate models, Sun et al. (2006) revealed two common biases in the AMIP runs of models: 1) an underestimate of the strength of the negative shortwave radiation forcing of clouds (SWCRF) feedback and 2) an overestimate of the positive feedback from the greenhouse effect of water vapor. Extending the same analysis to the fully coupled simulations of these models as well as other coupled models in CMIP3, Sun2009 found that these two biases persist. Studies by Lloyd et al. (2009, 2011, 2012) using CMIP3 outputs show that bias in the SWCRF feedback is the main source of model uncertainty and the biases in the cloud response to dynamical changes dominate the

modeled SWCRF feedback. The main purpose of present study is to update the results of Sun2009 using CMIP5 models, and specifically explore whether the newer models have improvements in simulating the two aforementioned feedbacks and the corresponding origins for the improvements.

The remainder of the paper is organized as follows. After describing the data and methods used in this study in Section 2, we show the changes and improvements from CMIP3 to CMIP5 in Section 3, particularly in reference to the key results from Sun2009. We then show the correlation among biases in different feedbacks and explore the causes for the biases in section 4. Finally, a summary and discussion is given in Section 5.

2. Data and Methodology

a. Model, Observational and Reanalysis Datasets

The model data are derived from CMIP5 multimodel dataset (Talor et al. 2012). Outputs from 18 CMIP5 models participating in the Intergovernmental Panel for Climate Change Fifth Assessment Report (IPCC AR5) are used in this study. Their acronyms and the names of the institution that have provided them to IPCC AR5 are listed in Table 1. The reason we chose these 18 models for our initial focus is that they are the models whose outputs including both historical runs and AMIP runs had been submitted to the Program for Climate Model Diagnosis and Intercomparison (PCMDI)

99 at the time of our analysis. The historical (AMIP) runs of these models cover the
100 period 1850-2005 (1979-2005).

101 The radiative fluxes supplied by the International Satellite Cloud Climatology
102 Project (ISCCP; Zhang et al. 2004) and the precipitation derived from the Global
103 Precipitation Climatology Project (GPCP; Huffman et al. 2009) data are used in this
104 study. In addition, the datasets including 1) Hadley Centre Sea Ice and Sea Surface
105 Temperature dataset (HadISST; Rayner et al. 2003) and 2) the US National Centers
106 for Environmental Prediction-Department of Energy reanalysis data (NCEP-DOE,
107 Kanamitsu et al. 2002) are also employed. As the surface heat fluxes of NCEP2 are
108 subject to larger errors in the eastern Pacific (Cronin et al. 2006), to provide a lower
109 bound to the uncertainty, the turbulent heat fluxes from OAFlux (Yu et al. 2007) are
110 employed to calculate the observed feedbacks associated with the surface heat flux. In
111 the present analysis, all the monthly datasets are analyzed during the period from
112 1984 to 2005 and have been interpolated to a common horizontal grid of 2.5°×2.5°.

113 *b. Analysis method*

114 In order to have a straight comparison with the results shown in Sun2009 and
115 showcase the improvements from CMIP3 to CMIP5 in the key feedbacks underscored
116 in Sun2009, the primary methodology used here is the same as that employed in
117 Sun2009: we obtain SSTA averaged over the equatorial Pacific (5°S-5°N,
118 150°E-110°W) by removing the monthly annual cycle of SST, and then calculate the

values of feedbacks during ENSO through a linear regression using the interannual variations of the SSTA and the corresponding variables. To obtain a more complete characterization of the model deficiencies and identify common factors responsible for the discrepancies in physical processes, we further introduce a skill score as an additional measure of the model deficiencies. In reference to the previous skill score formula for model performance (Taylor 2001; Hirota et al. 2011), the skill score in the present study is given by the following formula:

$$Skill\ Score = \frac{(1+R)^2}{(SDR + \frac{1}{SDR})^2} \qquad (1)$$

where R is a pattern correlation between the observation and the models, and SDR is the ratio of spatial standard deviations of the models against that of the observation. It is clear from equation (1) that both the spatial distribution and magnitude have been considered in this expression while comparing model results with observations.

3. Changes and Improvements from CMIP3 to CMIP5

a. Comparison of SWCRF feedback between CMIP3 and CMIP5

The feedbacks from cloud and water vapor to El Niño warming in CMIP5 models are presented in Table 2, that is the same as the Table 1 and Table 2 in Sun2009 except that the results are from 18 CMIP5 models, while the results in Sun2009 are based on 12 CMIP3 models. The ensemble model mean values for high

score models and low score models are also listed in Table 2 for later discussion.

As shown in column 1 of Table 2, nearly all the CMIP5 models still overestimate the positive feedback from the greenhouse effect of water vapor ($\frac{\partial(G_a)}{\partial T}$). The magnitude of the bias is similar to that was found in CMIP3 models. Although there are variations among models, CMIP5 models on average do not show significant improvements in their representation of the water vapor feedback. In contrast, the underestimate of the strength of the negative SWCRF feedback ($\frac{\partial(C_s)}{\partial T}$), emphasized in Sun2009, is notably alleviated in some of CMIP5 models. A striking improvement is noted in the NCAR and IAP models. Their CMIP5 version (CCSM4 and FGOALS-g2) now have a negative SWCRF feedback (-12.73 W m^{-2} K^{-1} and -14.46 W m^{-2} K^{-1} in the historical runs) that are very close to the observed value (-13.33 W m^{-2} K^{-1}), recalling that the values are respectively -3.69 W m^{-2} K^{-1} and -2.25 W m^{-2} K^{-1} in the coupled runs of CMIP3 version (CCSM3 and FGOALS-g1.0) (see Table 2). In addition, the SWCRF feedback in the historical runs of CCSM4, FGOALS-g2, GISS-E2-R and NorESM1-M, agree well with observations over the equatorial Pacific. This is also an encouraging improvement over CMIP3 models, in which nearly all of them have notable biases in simulating the SWCRF feedback (see the italicization in Table 2). However, the negative SWCRF feedback is still underestimated in the historical runs of more than half of CMIP5 models examined here. The numbers in the parenthesis in column 4 of Table 2 are the SWCRF feedback ($\frac{\partial(C_s)}{\partial T}$) estimated from the corresponding AMIP runs. It is evident that most CMIP5 models perform better in

simulating the SWCRF feedback in the AMIP runs than those in the historical runs.

As listed in the second column of Table 2, the positive feedback of longwave radiation forcing of clouds (LWCRF) is also underestimated in most models. But the magnitude of the biases from LWCRF does not appear to always compensate those in the feedback from water vapor and SWCRF, leading to diverse results among models in the feedback from the total greenhouse effect of water vapor and clouds ($G_a + C_l$) (colum3, Table 2) and the net clouds feedback ($C_l + C_s$) (column 5, Table 2). The feedback from the atmospheric transport ($\frac{\partial(D_a)}{\partial T}$), the net atmospheric feedback ($\frac{\partial(F_a)}{\partial T}$), and the feedback from the net surface heat flux into the ocean ($\frac{\partial(F_s)}{\partial T}$) are also listed in Table 2. In general, they show a slight improvement from the present CMIP5 models compared to the CMIP3 models (Sun2009).

b. Spatial structure of the feedbacks in El Niño Warming

Fig. 1 and Fig. 2 further show the spatial structure of the response of SWCRF to El Niño warming in the AMIP runs and the historical runs of CMIP5 models, respectively. The spatial distribution and magnitude of the response of SWCRF is generally captured well in most AMIP runs (Fig. 1). In reference to the results of Sun2009, the AMIP results show a slight improvement from CMIP3 to CMIP5. Comparisons with the observations also reveal that the simulation of SWCRF feedback in CMIP5 models performs better in the AMIP runs than those in the historical runs. Relative to the AMIP runs, the corresponding historical runs are found

178 to have a larger spread among models and a greater difference between models and
179 observations (Fig. 2). The most notable discrepancies with observations are the
180 location and magnitude of the maximum response of SWCRF. First, with a few
181 exceptions (i.e., ACCESS1-0, CCSM4, BCC-CSM1-1, FGOALS-g2, GISS-E2-R and
182 NorESM1-M), the maximum response of SWCRF has an obvious westward extension
183 in other models. Second, the maximum response of SWCRF is significantly
184 underestimated in most CMIP5 models except for CCSM4, CNRM-CM5,
185 FGOALS-g2, GISS-E2-R and NorESM1-M.

186 Compared to their corresponding AMIP runs, 9 out of the 18 CMIP5 models
187 examined here (i.e., CanESM2, CSIRO-Mk3-6-0, INMCM4, IPSL-CM5A-LR,
188 FGOALS-s2.0, MIROC5, the two MPI models and MRI-CGCM3) show that the
189 maximum response of SWCRF shifts westward in the historical runs. In addition, the
190 magnitude of maximum response of the SWCRF shown in the historical runs (Fig. 2)
191 has a general weakening in the response of SWCRF compared to their respective
192 AMIP results that show a better agreement with the observations (Fig. 1). This
193 common bias exists in more than half of the 18 CMIP5 models examined herein.

194 Overall, in terms of both the structure and magnitude, the AMIP simulations of
195 response of SWCRF to the El Niño warming in CMIP5 models show a slight
196 improvement over CMIP3 models. In addition, the performance in the historical runs
197 is significantly improved in about one third of CMIP5 models relative to CMIP3
198 results (Sun2009). Nonetheless, a large spread still exists among models, and the

biases in the representation of the cloud and water vapor feedbacks in the ENSO cycle are generally amplified in the historical runs compared to the corresponding AMIP runs.

4. An analysis of the origin of the biases

a. Relationship of biases among different feedbacks

For further evaluating model performance and revealing the origin of biases analyzed above, we have compared the skill scores of the feedbacks of SWCRF, LWCRF, precipitation, vertical velocity at 500 hPa (ω500) (Fig. 3). As is shown in Fig. 3a-c, there is a positive correlation between the inter-model variations in the simulated SWCRF feedback and the inter-model variations in other simulated feedbacks—the feedback of precipitation, the LWCRF feedback and the feedback of the large scale circulation (e.g., ω500). It is suggested that models with higher skill in simulating the response of SWCRF to El Niño warming generally perform better in other physical feedback processes (Fig. 3a, 3b and 3c). The apparent correlations among model biases imply that all the biases might be resulted from the same fundamental origins.

Hence, according to the skill in simulating the SWCRF feedback in the historical runs, we divide the 18 CMIP5 models into 2 categories: high score models (HSM) and low score models (LSM). The HSM, identified with the higher skill scores above 0.5 (see the models above the dashed line in Fig. 3d), includes 9 models: CCSM4, CNRM-CM5, NorESM1-M, FGOALS-g2, ACCESS1-0, BCC-CM1-1, BNU-ESM,

GISS-E2-R and HadGEM2-ES models (sorted by the score in the simulation of SWCRF feedback), and the LSM is identified with the lower skill scores below 0.5 (see the models below the dashed line in Fig. 3d). It is found that the ensemble of the HSM definitely performs better than the ensemble of the LSM in the historical runs over the tropical region (Fig. 2t and Fig. 2u). However, the difference between the HSM and the LSM in simulating the SWCRF feedback is smaller in the AMIP runs (see Fig. 1t, Fig. 1u, Fig. 2t and Fig. 2u). It suggests that a better representation of the SWCRF feedback in the AMIP runs cannot guarantee a better simulation in its historical counterpart (as shown in Fig. 3d). As shown in the last two rows of Table 2, the values of most feedback coefficients listed in Table 2 generally agree better with observations in the HSM than those in the LSM, even though only variations in the equatorial Pacific (5 ℃S-5 ℃N, 150 ℃E-110 ℃W) are used to obtain these values in Table 2.

b. Origins of the biases

Based on the results analyzed above, one may question what causes the biases of the cloud and water vapor feedbacks in models and significant differences between AMIP runs and historical runs.

When it comes to the improvement from CMIP3 models to the CMIP5 models in the historical runs, it is tempting to attribute the biases of the feedbacks to the biases of the simulation of ENSO. However, it is noted that a better simulation of ENSO variability is generally not accompanied by a more realistic SWCRF feedback to ENSO. Fig. 4 displays the relationship between the skill of reproducing ENSO

variability as measured by the ratio of the standard deviation (STD) of the simulated Niño3 SSTA over the STD of the observed Niño3 SSTA, and the skill in the corresponding SWCRF feedbacks in the historical runs. The red open circles and the blue open squares in the figure indicate the results from the HSM and the LSM respectively. The figure shows clearly that the higher skill score of SWCRF feedback is not necessarily accompanied by a better simulation of ENSO. For example, the CCSM4 model, which has overestimated the amplitude of ENSO, shows a well simulated SWCRF feedback in its historical runs. But the IPSL-CM5A-LR model, in which the ENSO amplitude is close to the observation, does not simulate the SWCRF feedback well. Therefore, the bias in the simulation of ENSO is unlikely a major factor behind the biases of feedbacks in the coupled GCMs.

The leading candidate for the feedback biases in the historical runs may be the excessive cold tongue in models (Sun et al. 2006, 2009). To test this hypothesis, we have examined the climatological mean tropical Pacific SST in the historical runs of the HSM and the LSM (Fig. 5b and Fig. 5c). Although the spatial pattern of the mean SST is similar to the observations, the cold bias in the equatorial Pacific appears in both the HSM and the LSM except the eastern equatorial Pacific, and the warm bias is prevalent adjacent to the Peru coast, which have been pointed out earlier and continue to exist in current coupled GCMs (Mechoso et al. 1995; Davey et al. 2002; Latif et al. 2001; Sun et al. 2006). Note that the bias of the climatological mean SST is generally smaller in the HSM than that in the LSM, especially over the central equatorial Pacific.

As we know, the deep convection tends to occur where SST is higher than a threshold around 28℃ (Graham and Barnett 1987) and the dependence of precipitation on SST is highly nonlinear (see Fig. 5a in Sun2009). Therefore the cold bias of SST in central equatorial Pacific may lead to a decrease in the precipitation over the central equatorial Pacific and shift the deep convection westward. By comparing the response of precipitation to El Niño warming in both AMIP and historical runs of two categories of models (figures not shown), it is found that the response of precipitation in the LSM historical runs is significantly weaker than that in observations and has a westward shift, whereas the response of precipitation in the HSM historical runs is slightly weaker and the location matches better with the observations. However, the precipitation feedback in the corresponding AMIP runs of both the HSM and the LSM are well simulated (the skill scores are 0.92 and 0.93). Recall that the AMIP runs are forced by the same observed SST, it thus suggests that the mean SST bias in the historical runs especially the excessive cold tongue may contribute to the underestimate of the SWCRF feedback and the westward shift of the maximum response of SWCRF.

To further test this hypothesis, we have examined the relationship between the cold-tongue biases and the skill scores of the SWCRF feedback in all the historical runs (Fig. 6). In Fig. 6, we use the mean SST bias over the equatorial Pacific (5°S-5°N, 150°E-110°W) as a measure of the cold-tongue bias. A colder SST bias in this region indicates a more excessive cold tongue. Fig. 6 shows that the models with smaller

cold-tongue biases are generally accompanied by the higher scores of the SWCRF feedback (i.e. the better simulation of the SWCRF feedback), implying that reducing the cold bias of the mean SST may be beneficial for the better simulation of the SWCRF feedback. Also note that most of the CMIP5 coupled models exhibit cold SST biases. Consistent with Fig.5, the models in the group of HSM generally exhibit smaller cold SST biases or even warm biases compared to the models in the LSM.

It should be noted, however, the excessive cold tongue in the models may in turn be affected by the biases in the net atmospheric feedbacks. According to Sun et al. (2003) (see their Fig. 6), the prevalence of the excessive cold tongue is possibly related to the incorrect representation of the net atmospheric feedbacks (i.e., $\partial(F_a)/\partial T = \partial(G_a)/\partial T + \partial(C_l)/\partial T + \partial(C_s)/\partial T + \partial(D_a)/\partial T$). Fig 7 shows the observed and model-simulated $\partial(F_a)/\partial T$ over the tropical Pacific. It is found that in the historical runs, $\partial(F_a)/\partial T$ from both the HSM and the LSM are much weaker than the observation (see Fig. 7b and Fig. 7c), and the latter is even weaker (note that this feedback in the LSM is barely negative over the central equatorial Pacific). Also as shown in the last second column of Table 2, $\partial(F_a)/\partial T$ over the equatorial Pacific (5°S-5°N, 150°E-110°W) in the HSM historical runs and the LSM historical runs are -7.23 ± 0.78 W m^{-2} K^{-1} and -0.31 ± 0.65 W m^{-2} K^{-1}, respectively. The latter feedback is much weaker than the former one. Therefore, the cold SST bias is less regulated by the atmospheric process in the coupled models, leading to the formation of an excessive cold tongue in these models. The excessive cold tongue then further

303 weakens the net atmospheric feedback. Such a vicious cycle may be a root cause for
304 the difficulty to make the equatorial Pacific cold tongue simulated correctly by
305 coupled GCMs.

306 Indeed, we find in our analysis that the air-sea interaction or coupling between
307 the atmosphere and ocean amplifies the errors in the atmospheric feedbacks. By
308 comparing the HSM and the LSM in the quantification of the skill scores over the
309 tropical Pacific (see Fig. 8), it is found that the simulated feedbacks in the AMIP
310 experiments are generally better than the historical experiments. Although the
311 representations of the feedbacks in the HSM AMIP runs are very close to those in the
312 LSM AMIP runs, they are very different in their corresponding historical runs. The
313 simulated feedbacks in the HSM historical runs are much better than those in the LSM
314 historical runs. Apparently, biases of the cloud and water vapor feedbacks in the LSM
315 AMIP runs are amplified more easily in their historical counterparts than those in the
316 HSM AMIP runs. This also implies that the improvements in the AMIP runs can have
317 an amplified gain in their corresponding coupled runs.

318 The persistence of the overestimated water vapor feedback in CMIP5 models is
319 linked with the bias of water vapor. As the greenhouse gases feedback is more
320 proportional to its percentage change (Shine and Sinha 1991; Schneider et al. 1999;
321 Zhang and Sun 2008), we have calculated the response of the specific humidity
322 change percentage (anomalies/mean) to El Niño warming in both the AMIP runs and
323 the historical runs of CMIP5 models in the same manner as Zhang and Sun (2006,

2008). We found the excessive response of water vapor in the upper troposphere in all models (figures not shown).

5. Summary and Discussion

Previous studies have revealed two common biases in the simulation of the response of the cloud and water vapor to the El Niño warming in CMIP3 models: an underestimate of the negative cloud albedo feedback and an overestimate of the positive water vapor feedback. To examine whether these two biases still exist in current climate models, we assessed the performances of CMIP5 models in representing these feedbacks. As indicated by the traditional feedback calculations as well as by a skill score designed for further evaluating the model simulations for the entire tropical Pacific, the major characteristics of the feedbacks from cloud and water vapor over the tropical Pacific regions in response to ENSO forcing are generally well captured by CMIP5 models. The skill in simulating the SWCRF feedback is found to be significantly higher in CMIP5 models than in CMIP3 models. The most impressive improvement in this regard was noted in the NCAR Climate System Model (Gent et al. 2011). Nevertheless, a large spread among models and a notable difference between the models and observations still exist in the historical runs of CMIP5 models. In addition, most of the CMIP5 models do not have significant improvements in simulating the water vapor feedback. More efforts need to be made to alleviate the positive bias in the water vapor feedback that still remains prevalent in CMIP5

344 models.

345 Given the fact that the biases from many other feedbacks correlate with the bias
346 in the SWCRF feedback, 18 CMIP5 models were further classified as the HSM and
347 the LSM according to their scores in simulating the SWCRF feedback in the historical
348 runs. By analyzing the differences of climatological mean tropical Pacific SST
349 between the HSM and the LSM, we reveal that the LSM tend to have a more severe
350 excessive cold tongue than HSM. Further analysis demonstrates that the excessive
351 cold tongue generally leads to a westward shift and a significant weakening of the
352 maximum response to El Niño warming. Among the coupled models, there is a
353 correlation between the cold bias in the equatorial cold-tongue and the bias in the
354 SWCRF feedback.

355 There are some improvements in the AMIP runs in simulating the SWCRF
356 feedback from CMIP3 models to CMIP5 models, but they remain small relative to the
357 inter-model differences. Nonetheless, understanding the causes for these
358 improvements is important as we have noted that a small gain in the AMIP runs
359 generally result in a much reduced bias in the coupled runs. Factors that are
360 potentially responsible for the improvements in the AMIP runs involve the improved
361 convection parameterization, the cloud micro-physics schemes and the model
362 resolutions (Zhang et al. 1998; Lin 2007; Li and G. J. Zhang 2008; Guilyardi et al.
363 2009; Lloyd et al. 2009, 2011, 2012). For example, there are some improvements of
364 SWCRF feedback in the atmospheric component model of FGOALS-g2 (named

GAMIL2) compared to its previous version (named GAMIL1) (Li et al. 2012a). It has been pointed out by Li et al. (2012b, submitted) that the biases of shortwave and longwave cloud forcing distribution are reduced in GAMIL2 and the strength of atmospheric response to El Niño warming (i.e., regression coefficient between Southern Oscillation Index (SOI) and Niño3 SSTA) is much closer to the observations than GAMIL1. The former arises from the updated cloud macro/micro-physics schemes and their coordination with other schemes (e.g., the convection parameterization). And the latter is related to the artificially amplified liquid water path (LWP) in GAMIL1, which leads to an unrealistic response of the SWCRF and other corresponding variables to ENSO cycle. To be sure, factors responsible for the improvements in AMIP runs may vary with models or be model dependent.

Acknowledgements. We would like to thank two anonymous reviewers for their constructive and insightful comments. The discussion with Dr. Li about the model FGOLAS-g2 is gratefully acknowledged. This study is jointly supported by the "Strategic Priority Research Program Climate Change: Carbon Budget and Relevant Issues" of the Chinese Academy of Sciences (Grant No. XDA05110301), and the National Key Program for Developing Basic Sciences Grant No. 2010CB950502, the US National Science Foundation Climate Dynamics Program under AGS 0852329 and by grants from NOAA office of global programs (MAPP and ESS). We also

385 acknowledge the modeling groups, the PCMDI and the World Climate Research
386 Program's (WCRP's) Working Group on Coupled Modeling (WGCM) for their roles
387 in making available the WCRP CMIP5 multimodel dataset. Support of this dataset is
388 provided by the Office of Science, U.S. Department of Energy.

389 **References**

390 Bony, S., and J.-L. Dufresne, 2005: Marine boundary layer clouds at the heart of
391 tropical cloud feedback uncertainties in climate models. *Geophys. Res. Lett.*, **32**,
392 L20806, doi:10.10292005GL023851.

393 ——, and Coauthors, 2006: How well do we understand and evaluate climate change
394 feedback processes? *J. Climate*, **19,** 3445–3482.

395 Cess, R. D., and Coauthors, 1990: Intercomparison and interpretation of climate
396 feedback processes in 19 atmospheric general circulation models. *J. Geophys.*
397 *Res.*, **95**, 16601–16615.

398 ——, and Coauthors, 1996: Cloud feedback in atmospheric general circulation
399 models: An update. *J. Geophys. Res.*, **101**, 12791–12794.

400 Cronin, M. F., N. A. Bond, C. W. Fairall, and R. A. Weller, 2006: Surface cloud
401 forcing in the east Pacific stratus deck/cold tongue/ITCZ complex. *J.*
402 *Climate*, **19**, 392–409.

403 Davey, M. K., and Coauthors, 2002: STOIC: A study of coupled model climatology
404 and variability in tropical ocean regions. *Climate Dyn.*, **18**, 403–420.

405 Gent, P. R., and Coauthors, 2011: The Community Climate System Model version 4. *J.*
406 *Climate*, **24**, 4973–4991.

407 Graham, N. E., and T. P. Barnett, 1987: Sea surface temperature, surface wind
408 divergence, and convection over tropical oceans. *Science*, **238,** 657–659.

Guilyardi E, P. Braconnot, F.-F. Jin, S. T. Kim, M. Kolasinski, T. Li, and I. Musat, 2009: Atmosphere feedbacks during ENSO in a coupled GCM with a modified atmospheric convection scheme. *J. Climate,* **22,** 5698–5718.

Harrison, E. F., P. Minnis, B. R. Barkstrom, V. Ramanathan, R. D. Cess, and G. G. Gibson, 1990: Seasonal variation of cloud radiative forcing derived from the Earth Radiation Budget Experiment. *J. Geophys. Res.*, **95,** 18 687–18 703.

Hartmann, D. L., and D. A. Short, 1980: On the use of Earth radiation budget statistics for studies of clouds and climate, *J. Atmos. Sci.*, **37**, 1233-1250.

Houghton, J. T., Y. Ding, D. J. Griggs, M. Noguer, P. J. van der Linden, X. Dai, K. Maskel, and C. A. Johnson, Eds., 2001: *Climate Change 2001: The Scientific Basis.* Cambridge University Press, 881 pp.

Hirota, N., Y. N. Takayabu, M. Watanabe, and M. Kimoto, 2011: Precipitation reproducibility over tropical oceans and its relationship to the double ITCZ problem in CMIP3 and MIROC5 climate models. *J. Climate,* **24,** 4859–4873.

Huffman, G. J., R. F. Adler, D. T. Bolvin, and G. Gu, 2009: Improving the global precipitation record: GPCP version 2.1. *Geophys. Res. Lett.*, **36**, L17808, doi:10.1029/2009GL040000.

Kanamitsu, M., W. Ebisuzaki, J. Woollen, S.-K. Yang, J. J. Hnilo, M. Fiorino, and G. L. Potter, 2002: NCEP–DOE AMIP-II Reanalysis (R-2). *Bull. Amer. Meteor. Soc.*, **83**, 1631–1643.

Kiehl, J. T., and K. E. Trenberth, 1997: Earth's annual global mean energy budget.

Bull. Amer. Meteor. Soc., **78**, 197–208.

Latif，and Coauthors, 2001: ENSIP: The El Niño simulation inter-comparison project. *Climate Dyn.,* **18,** 255–276.

Li, G. and G. J. Zhang, 2008: Understanding biases in shortwave cloud radiative forcing in the National Center for Atmospheric Research Community Atmosphere Model (CAM3) during El Niño. *J. Geophys. Res.,* **113,** D02103, doi:10.1029/2007JD08963.

Li, G. and G. J. Zhang, 2008: Understanding biases in shortwave cloud radiative forcing in the National Center for Atmospheric Research Community Atmosphere Model (CAM3) during El Niño. *J. Geophys. Res.*, **113,** D02103, doi:10.1029/2007JD08963.

Li Lijuan, and Coauthors, 2012a: The Flexible Global Ocean-Atmosphere-Land System Model: Grid-point Version 2: FGOASLS-g2. *Adv. Atmos. Sci.*, in press.

——, and Coauthors, 2012b: Development and Evaluation of grid-point Atmospheric Model of IAP LASG version 2 (GAMIL2). *Submitted to Adv. Atmos. Sci.*

Lin, J-L., 2007: The double-ITCZ problem in IPCC AR4 coupled GCMs: Ocean–atmosphere feedback analysis. *J. Climate*, **20,** 4497–4525.

Lloyd, J., E. Guilyardi, H. Weller, and J. Slingo, 2009: The role of atmosphere feedbacks during ENSO in the CMIP3 models. *Atmos. Sci. Lett.*, **10**, 170–176.

——, —— and ——, 2011: The role of atmosphere feedbacks during ENSO in the CMIP3 models. Part II: Using AMIP runs to understand the heat flux feedback

mechanisms. *Climate Dyn.*, **37**, 1271–1292.

——, —— and ——, 2012: The Role of Atmosphere Feedbacks during ENSO in the CMIP3 Models. Part III: The Shortwave Flux Feedback. *J. Climate*, **25**, 4275–4293.

Manabe, S., and R. T. Wetherald, 1967: Thermal equilibrium of the atmosphere with a given distribution of relative humidity. *J. Atmos. Sci.*, **24**, 241–259.

Mechoso, C. R., and Coauthors, 1995: The seasonal cycle over the tropical Pacific in coupled ocean–atmosphere general circulation models. *Mon. Wea. Rev.*, **123,** 2825–2838.

Randall, D. A., and Coauthors, 2007: Climate models and their evaluation. *Climate Change 2007: The Physical Science Basis.* S. Solomon et al., Eds., Cambridge University Press, 589–662.

Rayner, N. A., D. E. Parker, E. B. Horton, C. K. Folland, L. V. Alexander, D. P. Rowell, E. C. Kent, and A. Kaplan, 2003: Global analyses of sea surface temperature, sea ice, and night marine air temperature since the late nineteenth century. *J. Geophys. Res.*, **108**, 4407, doi:10.1029/2002JD002670.

Schneider, Edwin K., Ben P. Kirtman, Richard S. Lindzen, 1999: Tropospheric Water Vapor and Climate Sensitivity. *J. Atmos. Sci.*, **56**, 1649–1658.

Shine, K. P., and A. Sinha, 1991: Sensitivity of the Earth's climate to height dependent changes in the water vapor mixing ratio. *Nature,* **354,** 382–384.

Soden, B. J., 1997: Variations in the tropical greenhouse effect during El Niño. *J.*

Climate, **10**, 1050–1055.

——, and I. Held, 2006: An assessment of climate feedbacks in coupled ocean–atmosphere models. *J. Climate*, **19**, 3354–3360.

——, I. M. Held, R. Colman, K. M. Shell, J. T. Kiehl, and C. A. Shields, 2008: Quantifying climate feedbacks using radiative kernels. *J. Climate*, **21**, 3504–3520.

Stephens, G. L., 2005: Cloud feedbacks in the climate system: A critical review. *J. Climate*, **18,** 237–273.

Sun, D.-Z., and I. M. Held, 1996: A comparison of modeled and observed relationships between interannual variations of water vapor and temperature. *J. Climat*e, **9**, 665–675.

——, J. Fasullo, T. Zhang, and A. Roubicek, 2003: On the radiative and dynamical feedbacks over the equatorial Pacific cold tongue. *J. Climate*, **16**, 2425–2432.

——, and Coauthors, 2006: Radiative and dynamical feedbacks over the equatorial cold tongue: Results from nine atmospheric GCMs. *J. Climat*e, **19**, 4059–4074.

——, Y. Yu, and T. Zhang, 2009: Tropical water vapor and cloud feedbacks in climate models: A further assessment using coupled simulations. *J. Climate*, **22**, 1287–1304.

Taylor, K. E., 2001: Summarizing multiple aspects of model performance in a single diagram. *J. Geophys. Res.*, **106** (D7), 183–7192.

Taylor, K.E., R.J. Stouffer, G.A. Meehl, 2012: An Overview of CMIP5 and the

493 experiment design. *Bull. Amer. Meteor. Soc.*, **93**, 485-498.
494 Xie, Shang-Ping, Clara Deser, Gabriel A. Vecchi, Jian Ma, Haiyan Teng, Andrew T.
495 Wittenberg, 2010: Global Warming Pattern Formation: Sea Surface Temperature
496 and Rainfall*. *J. Climate*, **23**, 966–986.
497 Zhang, G. J., J. T. Kiehl, and P. J. Rasch, 1998: Response of climate simulation to a
498 new convective parameterization in the National Center for Atmospheric
499 Research Community Climate Model (CCM3). *J. Climate*, **11**, 2097-2115.
500 Zhang, T., and D. -Z. Sun, 2006: Response of water vapor and clouds to El Niño
501 warning in three National Center for Atmospheric Research atmospheric models.
502 *J. Geophys. Res.*, **111,** D17103, doi:10.1029/2005JD006700.
503 —— and ——, 2008: What Causes the Excessive Response of the Clear-Sky
504 Greenhouse Effect to El Niño Warming in the NCAR Community Atmosphere
505 Models? *J. Geophys. Res.*, **113**, D02108, doi:10.1029/2007JD009247.
506 Zhang, Y., W. B. Rossow, A. A. Lacis, V. Oinas, and M. I. Mishchenko, 2004:
507 Calculation of radiative fluxes from the surface to top of atmosphere based on
508 ISCCP and other global data sets: Refinements of the radiative transfer model
509 and the input data. *J. Geophys. Res.*, **109**, D19105, doi:10.1029/2003JD004457.
510 Zhu, P., J. J. Hack, J. T. Kiehl, and C. S. Bretherton, 2007: Climate sensitivity of
511 tropical and subtropical marine low cloud amount to ENSO and global warming
512 due to doubled CO2. *J. Geophys. Res.*, **112**, D17108,
513 doi:10.1029/2006JD008174.

514 **Table Captions**

515 **Table 1** List of CMIP5 models analyzed in this study.

516 **Table 2** Tropical cloud and water vapor feedbacks from observations and coupled
517 models: the water vapor feedback ($\frac{\partial(G_a)}{\partial T}$), the LWCRF feedback ($\frac{\partial(C_l)}{\partial T}$), the
518 SWCRF feedback ($\frac{\partial(C_s)}{\partial T}$), the feedback from the atmospheric transport ($\frac{\partial(D_a)}{\partial T}$), the
519 net atmospheric feedback ($\frac{\partial(F_a)}{\partial T} = \frac{\partial(G_a)}{\partial T} + \frac{\partial(C_l)}{\partial T} + \frac{\partial(C_s)}{\partial T} + \frac{\partial(D_a)}{\partial T}$), and the
520 feedback from the net surface heat flux into the ocean ($\frac{\partial(F_s)}{\partial T}$). The values of these
521 feedbacks are obtained through a linear regression using the interannual variations of
522 SSTA and the corresponding fluxes over the equatorial Pacific (5°S-5°N,
523 150°E-110°W). The results in the parentheses are obtained from the corresponding
524 AMIP runs. The values in the last two rows are ensemble model mean for two groups
525 of models—High Score Model (HSM) and Low Score Model (LSM). The definition
526 of HSM and LSM are provided in Section 4. Boldface indicates the results from the
527 models that are in the HSM. For convenient comparison, some results from CMIP3
528 models (derived from Table 2 in Sun2009) are also shown but with italicization.
529

Figure Captions

Fig. 1 Response of the shortwave cloud radiative forcing (SWCRF) to El Niño warming ($\frac{\partial(C_s)}{\partial T}$) (shading; units: W m^{-2} K^{-1}) for (a) the observations, (b)-(s) the AMIP runs of CMIP5 models, (t) the ensemble model mean of the HSM and (u) the ensemble model mean of the LSM. The labels at the top right corner are the models' scores for their simulation of the SWCRF feedback.

Fig. 2 Same as Fig. 1, but for the corresponding historical runs.

Fig. 3 Scatter diagrams (a)-(c) showing the relationship in the historical runs between the biases of: the SWCRF feedback and (a) the precipitation feedback, (b) the LWCRF feedback, and (c) the feedback from ω at 500 hPa in historical runs. (d) The relationship between the SWCRF feedback in AMIP runs and the SWCRF feedback in historical runs. The dashed line indicates the score value (0.5) used for sorting the models into two groups (ie, the HSM and the LSM). The red (blue) ones indicate the HSM (LSM).

FIG.4. Diagram displaying the relationship between the skill scores of the simulated SWCRF feedbacks and the standard deviation of Niño3 SSTA in the coupled runs. The radial distance from the origin is the ratio of the simulated Niño3 SSTA standard deviation against the observed. The red open circles indicate the results in the HSM and the blue open squares indicate the results in the LSM. The skill scores of the SWCRF feedback in the historical runs are given by the azimuthal position of the open circles. The red (blue) ones indicate the HSM (LSM).

Fig. 5 Tropical mean SST (shading; units: ℃) for (a) the observation, (b) the ensemble mean of the HSM, and (c) the ensemble mean of the LSM. (d) The differences in ensemble mean SST between the two groups (LSM－HSM), and the biases of (e) the HSM and (f) the LSM. All the model results are derived from the historical runs of CMIP5 models.

FIG.6 Scatter diagram showing the relationship between the skill score of the SWCRF feedback and the cold-tongue biases as measured by SST difference from the observations over the equatorial Pacific (5 ℃S-5 ℃N, 150 ℃E-110 ℃W) in the historical runs (units: ℃). The red (blue) ones indicate the HSM (LSM).

FIG.7. The net atmospheric feedback ($\frac{\partial(F_a)}{\partial T}$) (shading; units: W m^{-2} K^{-1}), which are derived from (a) OAFlux and ISCCP, (b) the HSM historical runs, (c) the LSM historical runs.

FIG.8. Scatter diagram showing the values of skill scores of various feedbacks for the AMIP and historical runs of the HSM and the LSM. The Ga, Cl, Ga+Cl, Cs and Fs on the X axis indicate the water vapor feedback ($\frac{\partial(G_a)}{\partial T}$), the LWCRF feedback ($\frac{\partial(C_l)}{\partial T}$), the feedback of the total greenhouse effect of water vapor and clouds ($\frac{\partial(G_a+C_l)}{\partial T}$), the SWCRF feedback ($\frac{\partial(C_s)}{\partial T}$) and the feedback from the net surface heat flux into the ocean ($\frac{\partial(F_s)}{\partial T}$), respectively. Note that coupling generally lowers the score of AMIP runs, and the LSM is more affected than the HSM by the coupling in their simualtion of the feedbacks.

571 **Table 1** List of CMIP5 models analyzed in this study.

Model	Institution
ACCESS1-0	CSIRO (Commonwealth Scientific and Industrial Research Organisation, Australia), and BOM (Bureau of Meteorology, Australia)
BCC-CSM1-1	Beijing Climate Center(BCC),China Meteorological Administration, China
BNU-ESM	GCESS, BNU, Beijing, China
CanESM2	CCCma (Canadian Centre for Climate Modeling and Analysis, Victoria, BC, Canada)
CCSM4	NCAR (National Center for Atmospheric Research) Boulder, CO, USA
CNRM-CM5	CNRM (Centre National de Recherches Meteorologiques, Meteo-France, Toulouse, France) and CERFACS (Centre Europeen de Recherches et de Formation Avancee en Calcul Scientifique, Toulouse, France)
CSIRO-Mk3-6-0	Australian Commonwealth Scientific and Industrial Research Organization (CSIRO) Marine and Atmospheric Research (Melbourne, Australia) in collaboration with the Queensland Climate Change Centre of Excellence (QCCCE) (Brisbane,

	Australia)
FGOALS-g2	IAP (Institute of Atmospheric Physics, Chinese Academy of Sciences, Beijing, China) and THU (Tsinghua University)
FGOALS-s2	IAP (Institute of Atmospheric Physics), CAS (Chinese Academy of Sciences), Beijing, China
GISS-E2-R	NASA/GISS (Goddard Institute for Space Studies) New York, NY
HadGEM2-ES	Met Office Hadley Centre, Fitzroy Road, Exeter, Devon, EX1 3PB, UK
INMCM4	INM (Institute for Numerical Mathematics, Moscow, Russia)
IPSL-CM5A-LR	IPSL (Institut Pierre Simon Laplace, Paris, France)
MIROC5	AORI (Atmosphere and Ocean Research Institute, The University of Tokyo, Chiba, Japan), NIES (National Institute for Environmental Studies, Ibaraki, Japan), JAMSTEC (Japan Agency for Marine-Earth Science and Technology, Kanagawa, Japan)
MPI-ESM-LR	Max Planck Institute for Meteorology
MPI-ESM-MR	Max Planck Institute for Meteorology
MRI-CGCM3	MRI (Meteorological Research Institute, Tsukuba, Japan)

NorESM1-M	Norwegian Climate Centre

572

573 **Table 2** Tropical cloud and water vapor feedbacks from observations and coupled models: the water vapor feedback ($\frac{\partial(G_a)}{\partial T}$), the LWCRF feedback
574 ($\frac{\partial(C_l)}{\partial T}$), the SWCRF feedback ($\frac{\partial(C_s)}{\partial T}$), the feedback from the atmospheric transport ($\frac{\partial(D_a)}{\partial T}$), the net atmospheric feedback
575 ($\frac{\partial(F_a)}{\partial T} = \frac{\partial(G_a)}{\partial T} + \frac{\partial(C_l)}{\partial T} + \frac{\partial(C_s)}{\partial T} + \frac{\partial(D_a)}{\partial T}$), and the feedback from the net surface heat flux into the ocean ($\frac{\partial(F_s)}{\partial T}$). The values of these feedbacks are
576 obtained through a linear regression using the interannual variations of SSTA and the corresponding fluxes over the equatorial Pacific (5°S-5°N,
577 150°E-110°W). The results in the parentheses are obtained from the corresponding AMIP runs. The values in the last two rows are ensemble model mean
578 for two groups of models—High Score Model (HSM) and Low Score Model (LSM). The definition of the HSM and the LSM are provided in Section 4.
579 Boldface indicates the results from the models that are in the HSM. For convenient comparison, some results from CMIP3 models (derived from Table 2 in
580 Sun2009) are also shown but with italicization.

581

Feedback(W m^{-2} K^{-1})

Name of process	$\frac{\partial(G_a)}{\partial T}$	$\frac{\partial(C_l)}{\partial T}$	$\frac{\partial(G_a+C_l)}{\partial T}$	$\frac{\partial(C_s)}{\partial T}$	$\frac{\partial(C_l+C_s)}{\partial T}$	$\frac{\partial(D_a)}{\partial T}$	$\frac{\partial(F_a)}{\partial T}$	$\frac{\partial(F_s)}{\partial T}$
Observation	6.61 ±0.29	12.64 ±0.48	19.25 ±0.61	-13.33 ±0.68	-0.68 ±0.36	-20.28 ±1.01	-14.36 ±1.20	-21.43 ±1.04
ACCESS1-0	**9.18 ±0.29**	**10.53 ±0.48**	**19.71 ±0.73**	**-9.16 ±0.56**	**1.38 ±0.25**	**-17.57 ±0.91**	**-7.02 ±0.89**	**-12.21 ±0.93**
	(9.96 ±0.26)	**(12.33 ±0.51)**	**(22.29 ±0.73)**	**(-11.73 ±0.60)**	**(0.60 ±0.26)**	**(-23.05 ±0.93)**	**(-12.48 ±0.95)**	**(-19.00 ±0.98)**
BCC-CSM1-1	**7.74 ±0.15**	**8.37 ±0.36**	**16.11 ±0.46**	**-5.48 ±0.42**	**2.89 ±0.27**	**-16.36 ±0.81**	**-5.73 ±0.83**	**-12.74 ±0.90**
	(5.99 ±0.14)	**(7.76 ±0.39)**	**(13.74 ±0.49)**	**(-8.67 ±0.54)**	**(-0.91 ±0.35)**	**(-20.29 ±0.78)**	**(-15.22 ±0.88)**	**(-22.16 ±0.93)**
BNU-ESM	**8.95 ±0.11**	**9.54 ±0.28**	**18.49 ±0.38**	**-7.01 ±0.48**	**2.53 ±0.26**	**-15.64 ±0.49**	**-4.16 ±0.62**	**-10.45 ±0.64**
	(9.11 ±0.18)	**(12.53 ±0.44)**	**(21.65 ±0.59)**	**(-12.74 ±0.69)**	**(-0.21 ±0.37)**	**(-22.91 ±1.03)**	**(-14.01 ±1.23)**	**(-20.13 ±1.23)**
CanESM2	8.48 ±0.14	9.35 ±0.38	17.83 ±0.50	-1.47 ±0.41	7.88 ±0.25	-17.60 ±0.71	-1.23 ±0.63	-7.09 ±0.64
	(10.54 ±0.22)	(14.97 ±0.56)	(25.50 ±0.73)	(-10.48 ±0.75)	(4.48 ±0.38)	(-24.47 ±0.93)	(-9.45 ±0.98)	(-16.11 ±1.00)
CCSM4	**9.16 ±0.13**	**11.86 ±0.35**	**21.01 ±0.44**	**-12.73 ±0.43**	**-0.88 ±0.23**	**-15.25 ±0.58**	**-6.97 ±0.61**	**-13.33 ±0.64**
	(9.20 ±0.20)	**(13.47 ±0.53)**	**(22.67 ±0.67)**	**(-14.15 ±0.72)**	**(-0.68 ±0.45)**	**(-18.12 ±0.87)**	**(-9.60 ±0.97)**	**(-16.45 ±1.01)**
CCSM3	*8.95 ±0.15*	*10.26 ±0.47*	*19.21 ±0.57*	*-3.69 ±0.58*	*6.57 ±0.38*	*-8.50 ±0.54*	*7.02 ±0.49*	*-0.32 ±0.51*
	(10.18 ±0.19)	*(12.93 ±0.51)*	*(21.11 ±0.63)*	*(-10.31 ±0.63)*	*(-2.62 ±0.42)*	*(-5.39 ±0.80)*	*(7.42 ±0.83)*	*(0.42 ±0.83)*
CNRM-CM5	**9.44 ±0.17**	**9.70 ±0.30**	**19.14 ±0.44**	**-17.95 ±0.57**	**-8.25 ±0.33**	**-13.55 ±0.73**	**-12.36 ±0.84**	**-18.40 ±0.86**

CNRM-CM3	**(8.24 ±0.19)** *7.97 ±0.10* *(10.30 ±0.25)*	**(9.49 ±0.35)** *8.21 ±0.30* *(13.74 ±0.67)*	**(17.73 ±0.50)** *16.18 ±0.40* *(24.04 ±0.89)*	**(-17.93 ±0.62)** *-9.53 ±0.48* *(-20.21 ±0.94)*	**(-8.44 ±0.38)** *-1.32 ±0.27* *(-6.47 ±0.54)*	**(-19.67 ±1.15)** *-7.67 ±0.48* *(-10.82 ±1.22)*	**(-19.87 ±1.30)** *-1.03 ±0.56* *(-6.99 ±1.25)*	**(-26.31 ±1.30)** *-4.71 ±0.49* *(-8.82 ±1.11)*
CSIRO-Mk3-6-0	7.30 ±0.15 (9.84 ±0.23)	7.35 ±0.32 (11.10 ±0.50)	14.66 ±0.41 (20.93 ±0.69)	2.92 ±0.34 (-0.60 ±0.36)	10.28 ±0.28 (10.50 ±0.37)	-13.45 ±0.67 (-6.33 ±0.69)	4.14 ±0.67 (14.01 ±0.59)	-2.06 ±0.70 (7.62 ±0.61)
FGOALS-g2 *FGLALS-g1*	**6.72 ±0.09** **(6.26 ±0.16)** *7.84 ±0.04* *(N/A)*	**8.52 ±0.24** **(6.51 ±0.26)** *7.22 ±0.13* *(N/A)*	**15.24 ±0.70** **(12.77 ±0.38)** *15.16 ±0.16* *(N/A)*	**-14.46 ±0.40** **(-10.43 ±0.49)** *-2.25 ±0.12* *(N/A)*	**-5.95 ±0.33** **(-3.91 ±0.38)** *-5.08 ±0.08* *(N/A)*	**-16.65 ±0.47** **(-17.13 ±0.74)** *-12.55 ±0.23* *(N/A)*	**-15.88 ±0.75** **(-14.79 ±0.97)** *-0.36 ±0.20* *(N/A)*	**-20.96 ±0.88** **(-20.90 ±0.97)** *-6.11 ±0.20* *(N/A)*
FGOALS-s2	9.50 ±0.18 (9.85 ±0.26)	5.59 ±0.24 (6.19 ±0.35)	15.09 ±0.39 (16.04 ±0.55)	-1.49 ±0.59 (-7.41 ±0.86)	4.10 ±0.45 (-1.23 ±0.61)	-18.66 ±0.64 (-22.16 ±0.92)	-5.06 ±0.80 (-13.53 ±1.06)	-9.73 ±0.84 (-20.28 ±1.12)
GISS-E2-R *GISS-EH*	**9.86 ±0.27** **(9.46 ±0.22)** *7.07 ±0.24* *(N/A)*	**10.76 ±0.48** **(9.19 ±0.29)** *0.54 ±0.36* *(N/A)*	**20.61 ±0.71** **(18.65 ±0.47)** *7.61 ±0.47* *(N/A)*	**-10.56 ±0.42** **(-9.91 ±0.33)** *1.70 ±0.58* *(N/A)*	**0.19 ±0.34** **(-0.72 ±0.26)** *2.25 ±0.50* *(N/A)*	**-15.86 ±0.90** **(-15.70 ±0.80)** *N/A* *(N/A)*	**-5.81 ±0.79** **(-6.96 ±0.76)** *N/A* *(N/A)*	**-10.13 ±0.84** **(-14.03 ±0.82)** *N/A* *(N/A)*
HadGEM2-ES	**8.77 ±0.24**	**8.44 ±0.41**	**17.21 ±0.60**	**-2.40 ±0.57**	**6.04 ±0.31**	**-15.72 ±0.79**	**-0.91 ±0.81**	**-6.44 ±0.83**

	(9.43 ±0.25)	**(11.44 ±0.47)**	**(20.87 ±0.68)**	**(-11.06 ±0.54)**	**(0.39 ±0.24)**	**(-22.33 ±0.91)**	**(-12.51 ±0.91)**	**(-18.99 ±0.96)**
HadGEM1	*5.95 ±0.21*	*1.95 ±0.19*	*7.90 ±0.37*	*3.80 ±0.44*	*5.75 ±0.36*	*-5.70 ±0.52*	*6.00 ±0.69*	*-0.39 ±0.67*
	(11.06 ±0.31)	*(14.14 ±0.57)*	*(25.21 ±0.85)*	*(-14.02 ±0.68)*	*(-0.13 ±0.24)*	*(N/A)*	*(N/A)*	*(N/A)*
INMCM4	8.96 ±0.19	3.51 ±0.26	12.47 ±0.40	0.60 ±0.55	4.12 ±0.37	-11.07 ±0.53	2.00 ±0.67	-4.15 ±0.66
	(8.34 ±0.16)	(6.08 ±0.29)	(14.42 ±0.41)	(-7.03 ±0.52)	(-0.95 ±0.31)	(-17.67 ±0.68)	(-10.29 ±0.79)	(-16.62 ±0.79)
IPSL-CM5A-LR	7.52 ±0.11	6.77 ±0.46	14.29 ±0.53	0.26 ±0.35	7.03 ±0.24	-11.32 ±0.60	3.23 ±0.46	-2.50 ±0.47
	(9.68 ±0.17)	(13.44 ±0.69)	(23.13 ±0.78)	(-8.17 ±0.69)	(5.28 ±0.40)	(-17.89 ±0.96)	(-2.93 ±0.85)	(-9.29 ±0.87)
IPSL-CM4	*9.40 ±0.11*	*13.07 ±0.46*	*22.47 ±0.51*	*-9.56 ±0.54*	*3.51 ±0.33*	*-18.09 ±0.60*	*-5.18 ±0.61*	*-11.66 ±0.59*
	(9.66 ±0.15)	*(16.26 ±0.50)*	*(25.92 ±0.59)*	*(-13.94 ±0.62)*	*(2.32 ±0.33)*	*(-19.52 ±0.65)*	*(-7.53 ±0.65)*	*(-13.63 ±0.64)*
MIROC5	8.65 ±0.12	9.57 ±0.26	18.22 ±0.37	-6.75 ±0.23	2.82 ±0.15	-15.76 ±0.50	-4.30 ±0.46	-10.53 ±0.47
	(9.16 ±0.19)	(9.69 ±0.45)	(18.85 ±0.59)	(-6.16 ±0.42)	(3.53 ±0.27)	(-15.50 ±1.19)	(-2.81 ±1.13)	(-9.33 ±1.16)
MIROC3.2(hires)	*7.47 ±0.20*	*8.76 ±0.52*	*16.23 ±0.68*	*-1.32 ±0.56*	*7.45 ±0.30*	*-18.20 ±0.75*	*-3.28 ±0.69*	*-8.78 ±0.69*
	(7.99 ±0.13)	*(10.58 ±0.36)*	*(18.58 ±0.46)*	*(-4.21 ±0.46)*	*(6.38 ±0.24)*	*(-19.93 ±0.69)*	*(-5.57 ±0.74)*	*(-10.56 ±0.68)*
MPI-ESM-LR	6.63 ±0.15	4.91 ±0.25	11.54 ±0.37	-3.41 ±0.31	1.49 ±0.19	-10.59 ±0.47	-2.47 ±0.43	-7.40 ±0.44
	(9.61 ±0.25)	(13.22 ±0.57)	(22.84 ±0.77)	(-12.25 ±0.64)	(0.97 ±0.29)	(-22.67 ±1.18)	(-12.08 ±1.19)	(-18.70 ±1.23)
MPI-ESM-MR	7.28 ±0.24	4.37 ±0.37	11.64 ±0.57	-3.54 ±0.45	0.82 ±0.26	-9.08 ±0.75	-0.98 ±0.64	-6.26 ±0.70

ECHAM5/MPI	(9.62 ±0.24) *7.90 ±0.13* *(10.56 ±0.25)*	(12.27 ±0.50) *6.77 ±0.28* *(17.15 ±0.65)*	(21.89 ±0.68) *14.67 ±0.39* *(27.71 ±0.87)*	(-11.82 ±0.61) *-4.37 ±0.44* *(-20.31 ±1.01)*	(0.45 ±0.30) *2.40 ±0.23* *(-3.16 ±0.52)*	(-21.32 ±1.08) *-14.62 ±0.49* *(-27.20 ±1.08)*	(-11.24 ±1.10) *-4.32 ±0.54* *(-19.80 ±1.30)*	(-17.86 ±1.11) *-10.33 ±0.52* *(-24.81 ±1.25)*
MRI-CGCM3	8.57 ±0.24 (8.94 ±0.22)	7.10 ±0.43 (10.33 ±0.44)	15.68 ±0.62 (19.27 ±0.61)	1.51 ±0.68 (-9.15 ±0.63)	8.61 ±0.46 (1.18 ±0.36)	-15.30 ±0.91 (-20.89 ±0.94)	1.89 ±1.05 (-10.77 ±1.06)	-4.23 ±1.07 (-17.08 ±1.07)
NorESM1-M	**9.98 ±0.19** **(10.20 ±0.22)**	**13.51 ±0.58** **(13.98 ±0.67)**	**23.49 ±0.70** **(24.19 ±0.82)**	**-14.27 ±0.68** **(-13.80 ±0.84)**	**-7.60 ±0.41** **(0.19 ±0.49)**	**-15.41 ±0.78** **(-13.96 ±0.96)**	**-6.19 ±0.84** **(-3.57 ±1.08)**	**-11.44 ±0.87** **(-10.12 ±1.09)**
HSM	**8.87 ±0.18** **(8.65 ±0.20)**	**10.14 ±0.39** **(10.74 ±0.43)**	**19.00 ±0.57** **(19.40 ±0.59)**	**-10.45 ±0.50** **(-12.27 ±0.60)**	**-1.07 ±0.30** **(-1.52 ±0.35)**	**-15.78 ±0.72** **(-19.24 ±0.91)**	**-7.23 ±0.78** **(-12.11 ±1.01)**	**-12.90 ±0.82** **(-18.68 ±1.03)**
LSM	8.10 ±0.17 (9.51 ±0.22)	6.50 ±0.33 (10.81 ±0.48)	14.60 ±0.46 (20.32 ±0.65)	-1.26 ±0.43 (-8.12 ±0.61)	5.24 ±0.29 (2.69 ±0.37)	-13.65 ±0.64 (-18.77 ±0.95)	-0.31 ±0.65 (-6.57 ±0.97)	-6.00 ±0.67 (-13.07 ±1.00)

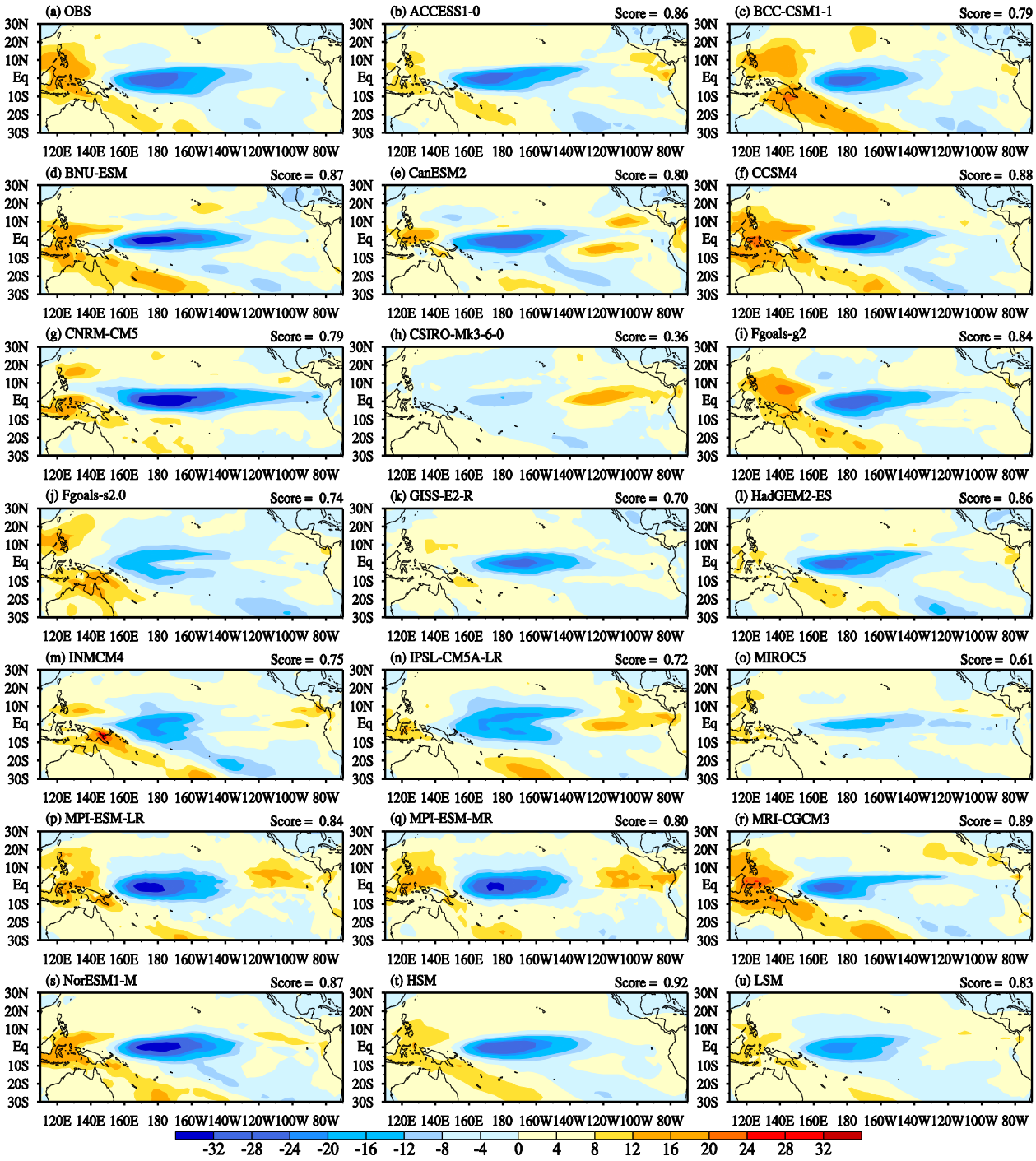

582

583 FIG.1. Response of the shortwave cloud radiative forcing (SWCRF) to El Niño warming ($\frac{\partial(C_s)}{\partial T}$)

584 (shading; units: W m^{-2} K^{-1}) for (a) the observations, (b)-(s) the AMIP runs of CMIP5 models, (t) the

585 ensemble model mean of the HSM and (u) the ensemble model mean of the LSM. The labels at the top

586 right corner are the models' scores for their simulation of the SWCRF feedback.

587

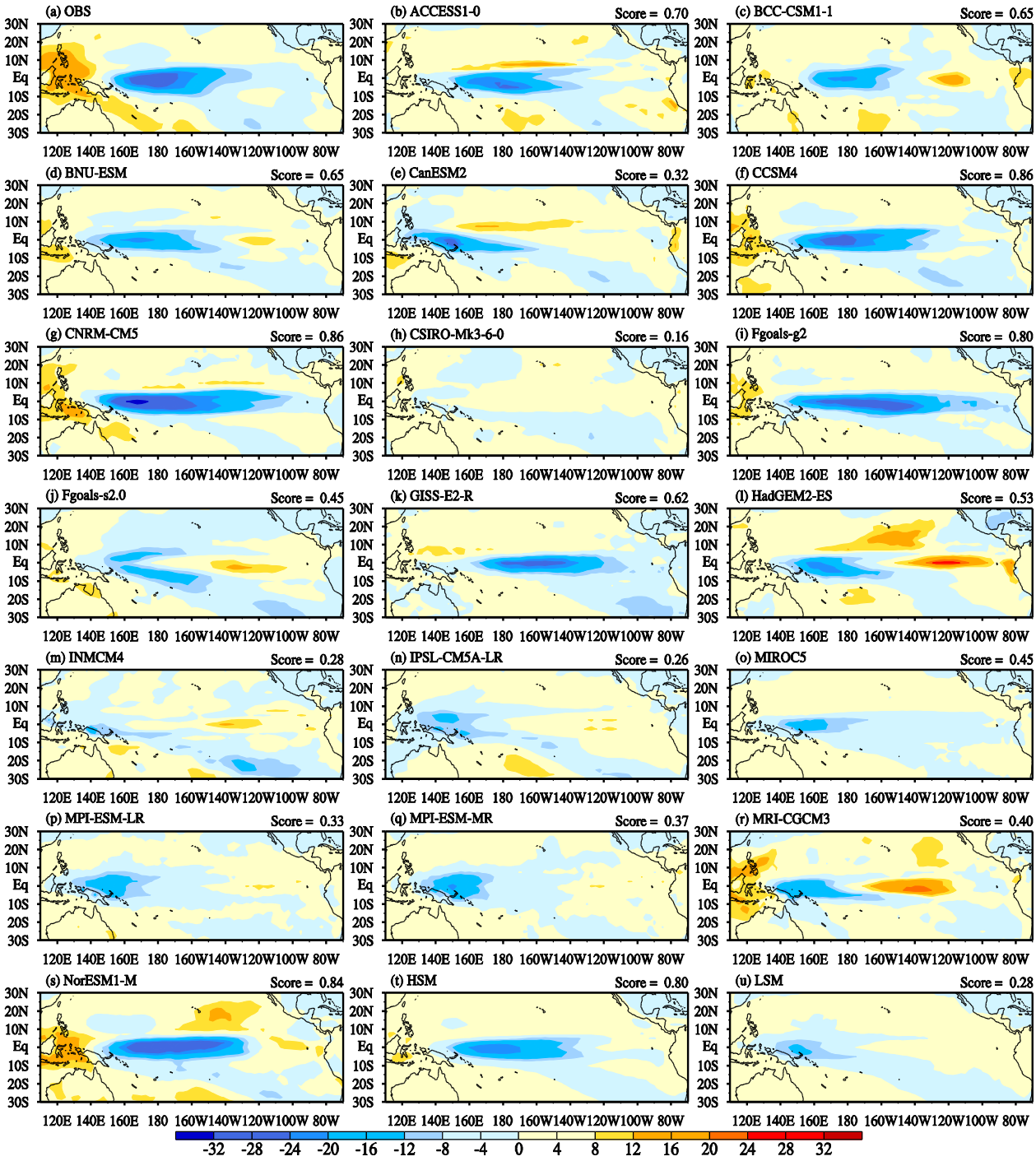

588

589 FIG.2. Same as Fig. 1, but for the corresponding historical runs.

590

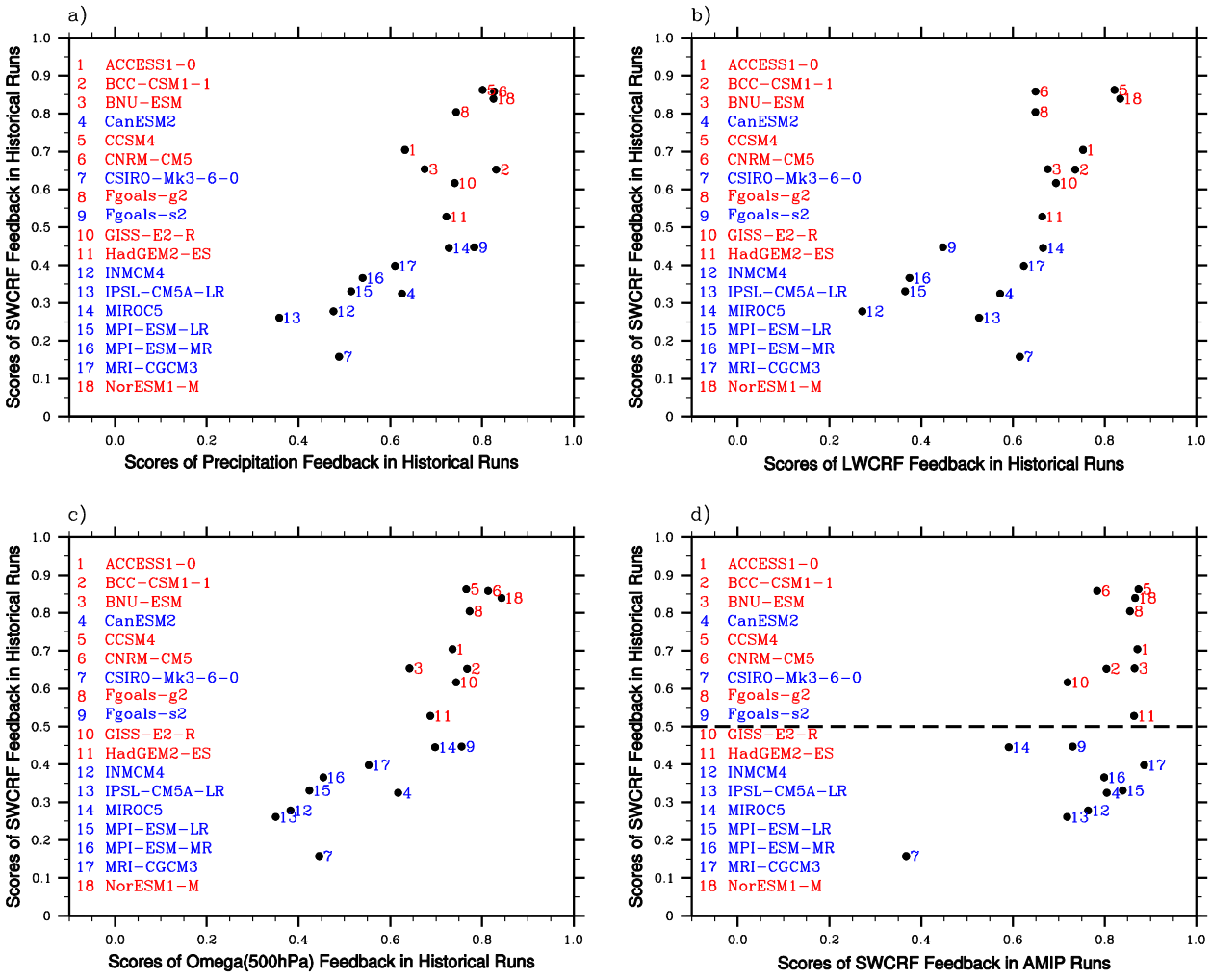

FIG.3. Scatter diagrams (a)-(c) showing the relationship in the historical runs between the biases of: the SWCRF feedback and (a) the precipitation feedback, (b) the LWCRF feedback, and (c) the feedback from ω at 500 hPa in historical runs. (d) The relationship between the SWCRF feedback in AMIP runs and that in historical runs. The dashed line indicates the score value (0.5) used for sorting the models into two groups (ie, the HSM and the LSM). The red (blue) ones indicate the HSM (LSM).

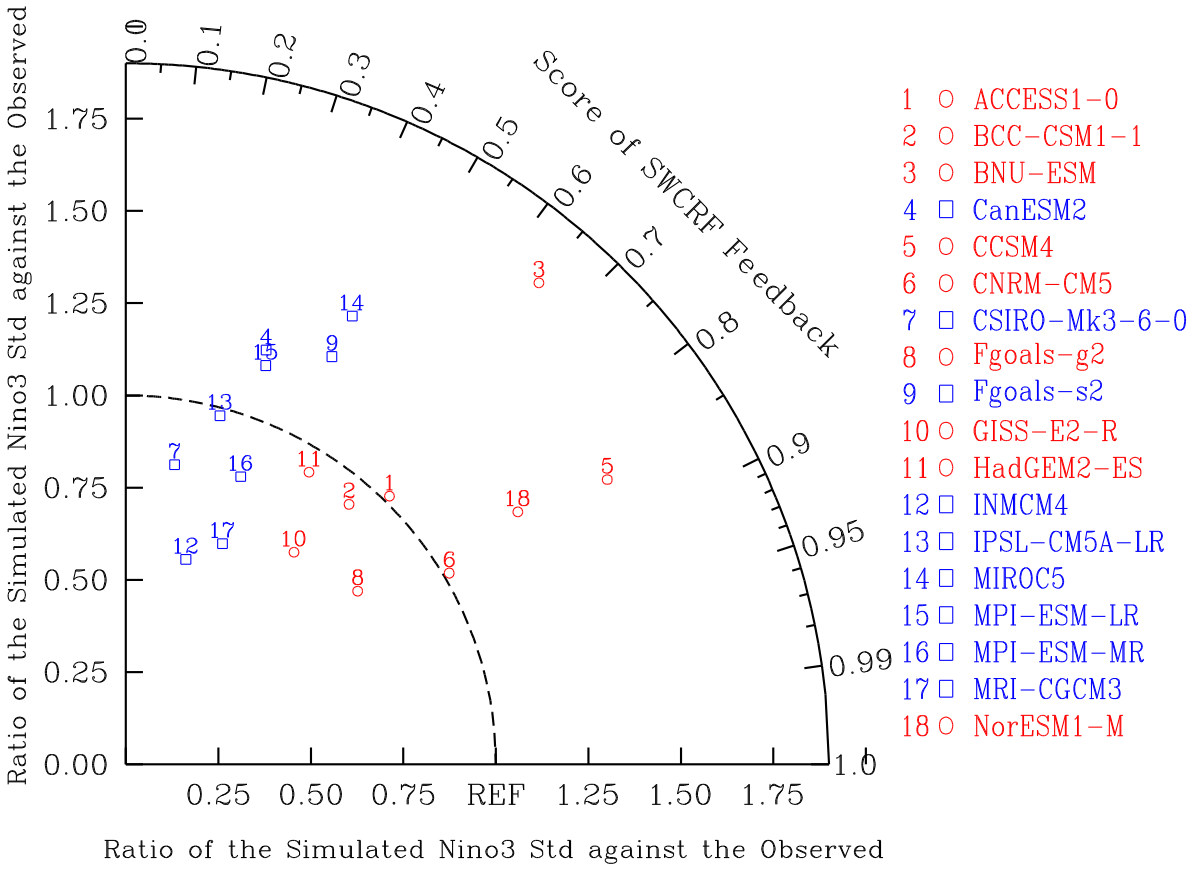

599

600

601 FIG.4. Diagram displaying the relationship between the skill scores of the simulated SWCRF feedbacks

602 and the standard deviation of Niño3 SSTA in the coupled runs. The radial distance from the origin is the

603 ratio of the simulated Niño3 SSTA standard deviation against the observed. The red open circles indicate

604 the results in the HSM and the blue open squares indicate the results in the LSM. The skill scores of the

605 SWCRF feedback in the historical runs are given by the azimuthal position of the open circles. The red

606 (blue) ones indicate the HSM (LSM).

607

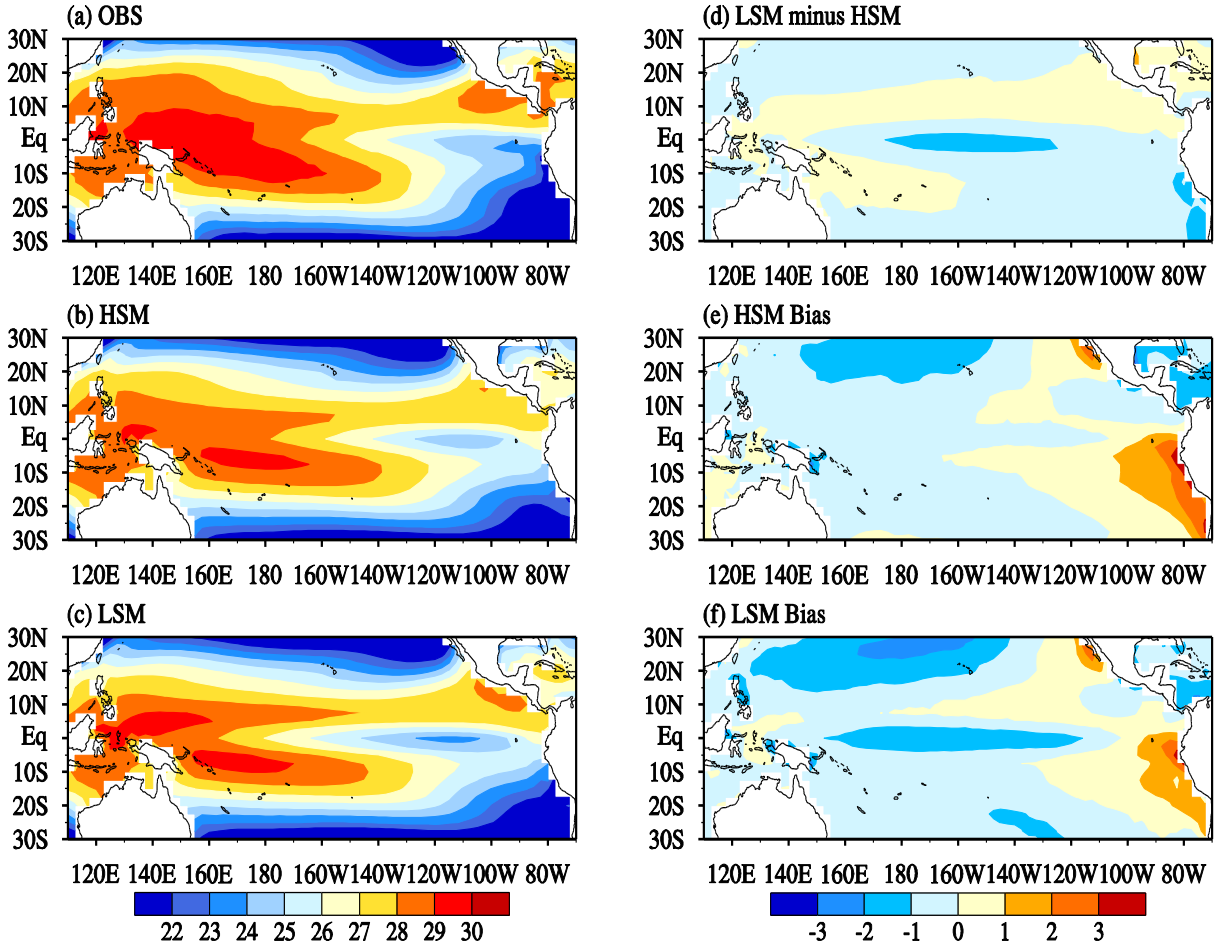

608

609 FIG.5. Tropical mean SST (shading; units: ℃) for (a) the observation, (b) the ensemble mean of the

610 HSM, and (c) the ensemble mean of the LSM. (d) The differences in ensemble mean SST between the

611 two groups (LSM－HSM), and the biases of (e) the HSM and (f) the LSM. All the model results are

612 derived from the historical runs of CMIP5 models.

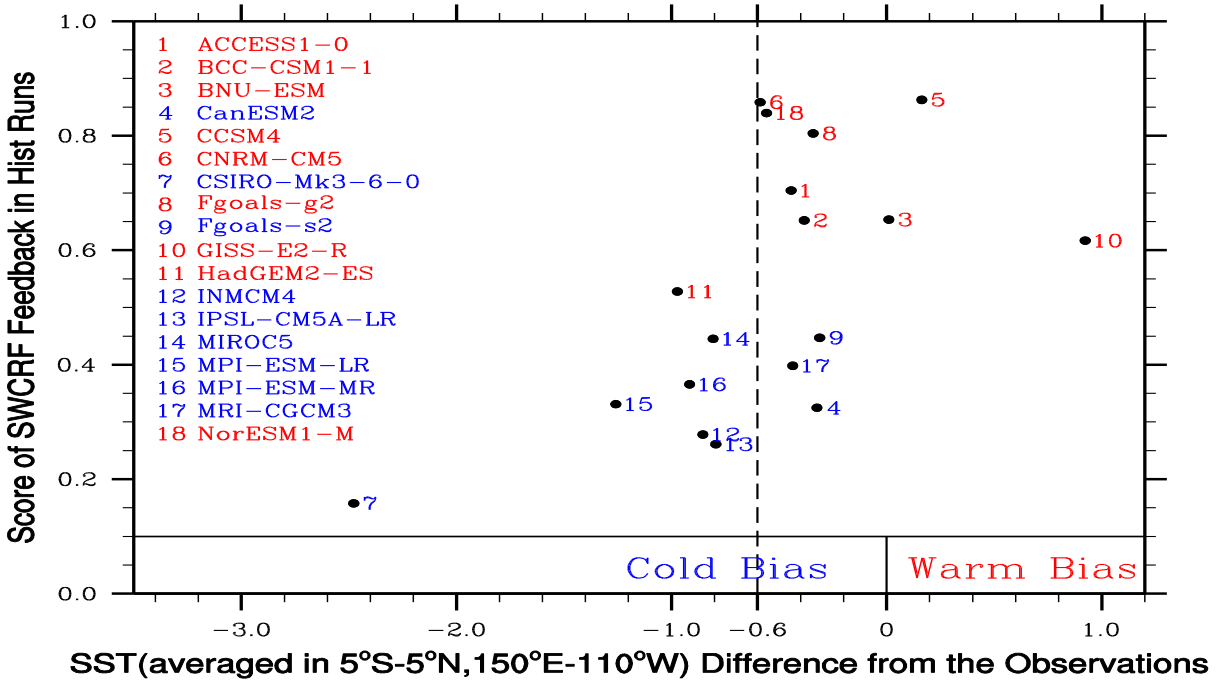

FIG.6. Scatter diagram showing the relationship between the skill score of the SWCRF feedback and the cold-tongue biases as measured by SST difference from the observations over the equatorial Pacific (5 ℃S-5 ℃N, 150 ℃E-110 ℃W) in the historical runs (units: ℃). The red (blue) ones indicate the HSM (LSM).

619

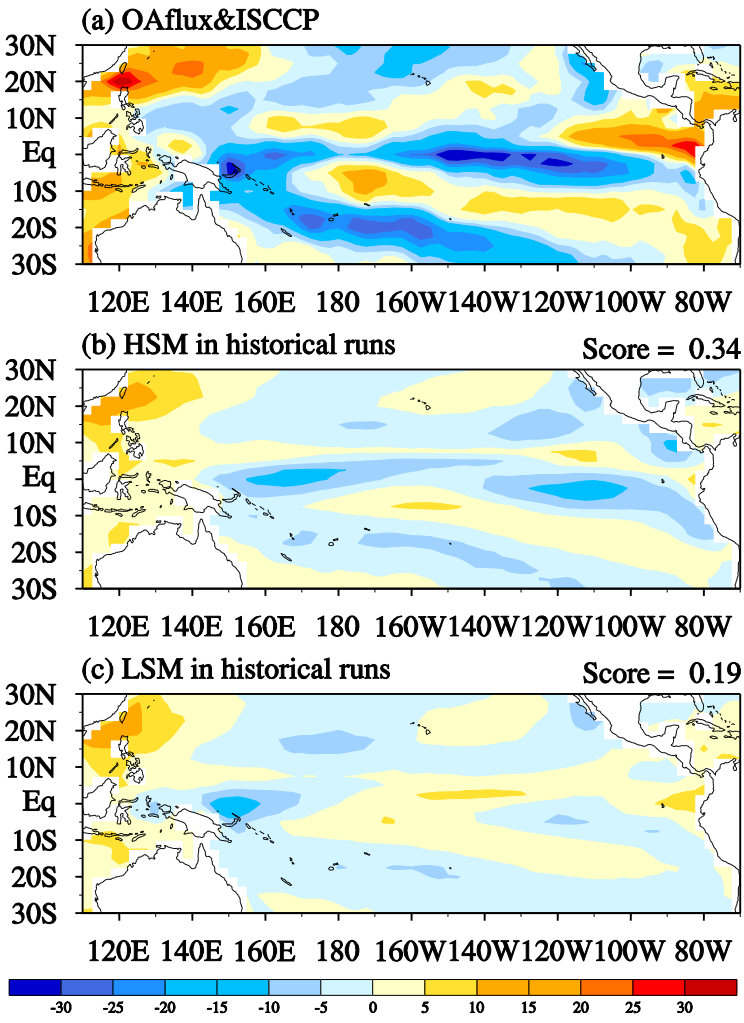

620

621 FIG.7. The net atmospheric feedback ($\frac{\partial(F_a)}{\partial T}$) (shading; units: W m^{-2} K^{-1}), which are derived from (a)

622 OAFlux and ISCCP, (b) the HSM historical runs, (c) the LSM historical runs.

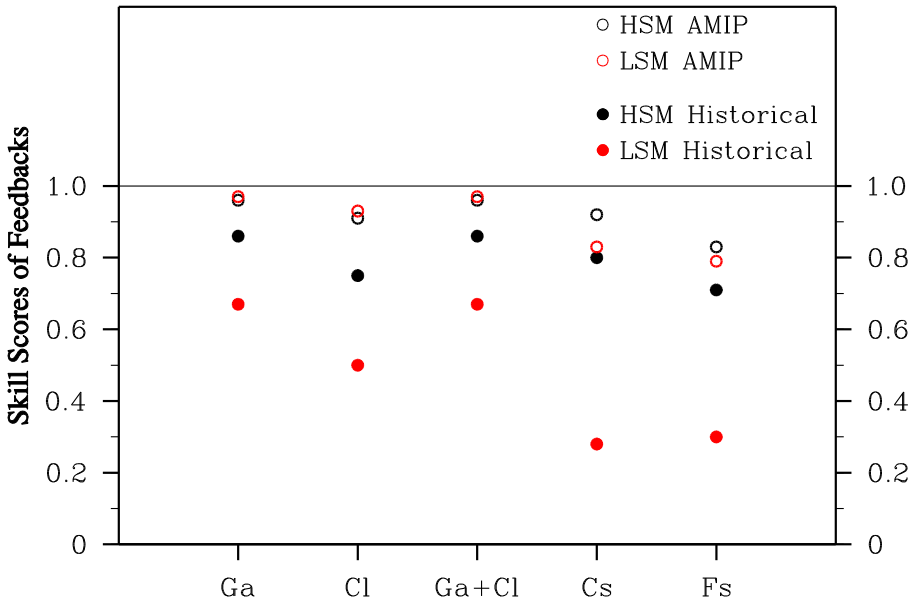

623

624 FIG.8. Scatter diagram showing the values of skill scores of various feedbacks for the AMIP and

625 historical runs of the HSM and the LSM. The Ga, Cl, Ga+Cl, Cs and Fs on the X axis indicate the water

626 vapor feedback ($\frac{\partial(G_a)}{\partial T}$), the LWCRF feedback ($\frac{\partial(C_l)}{\partial T}$), the feedback of the total greenhouse effect of

627 water vapor and clouds ($\frac{\partial(G_a+C_l)}{\partial T}$), the SWCRF feedback ($\frac{\partial(C_s)}{\partial T}$) and the feedback from the net

628 surface heat flux into the ocean ($\frac{\partial(F_s)}{\partial T}$), respectively. Note that coupling generally lowers the score of

629 AMIP runs, and the LSM is more affected than the HSM by the coupling in their simualtion of the

630 feedbacks.